

Intelligent aerospace structures with solid state sensors and actuators

Gangbing Song, Matthew A. Franchek, Karolos Grigoriadis, David Zimmerman, James B. Dabney, and Thomas L. Harman

ABSTRACT—This report presents results of research collaboration among scientists at the University of Houston’s central and Clear Lake campuses on intelligent solid-state materials such as piezoceramic sensors and actuators and their applications for vibration control. The report discusses active gravity gradient stabilization; increasing noise transmission loss using piezoceramic actuators; numerical analysis of acoustic wave propagation in carbon nanofiber composites; fuzzy logic-based active vibration control of smart beams with mass uncertainty; and vibration demonstration and active vibration control of a smart flexible beam.

I. ACTIVE GRAVITY GRADIENT STABILIZATION

Background

Gravity gradient stabilization is an attractive means of achieving satellite attitude control because it does not require any power or propulsion in its passive form.¹ The principle behind gravity gradient stabilization is that gravitational force between two bodies (such as the Earth and a satellite) varies inversely with the square of the distance between the two objects, forming a radial gravity gradient. If the longitudinal axis of a slender orbiting body (typically a satellite with a long boom supporting a distal mass) is not aligned with local vertical, the gravitational force exerted on the portion of the body closer to the Earth is greater than the gravitational force exerted on the portion farther from the Earth, resulting in a torque that tends to align the longitudinal axis with local vertical. In the case of a rigid satellite, there is very little damping in the system, giving rise to a periodic pendulum-like motion called libration. In the case of very long booms (idealized as rigid tethers), it is known that rapid attenuation of the libration (both in the orbital plane and normal to the orbital plane) can be achieved by actively moving the mass at the end of the boom out when angular velocity is high and in when angular velocity is low (yo-yo stabilization).²

Research tasks

While passive gravity gradient stabilization has been used for many years, active gravity gradient stabilization has been used primarily on tethered satellite systems. Although the technique is attractive in terms of simplicity and energy efficiency, several research issues must be addressed. First, relatively short booms (meters in length) produce much lower torques than tethers (thousands of meters in length). Therefore, it will be necessary to design booms such that the available stabilizing torque exceeds disturbance torques. Secondly, yo-

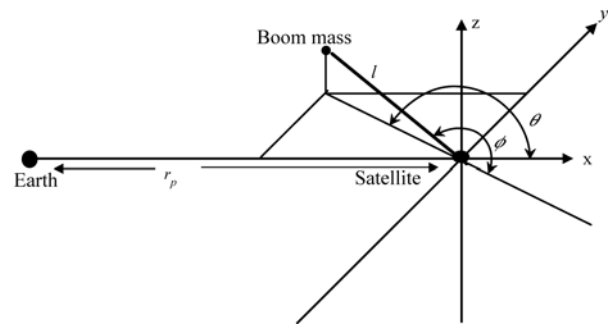


Figure 1.1. Satellite configuration

yo stabilization of tethered satellites typically involves moving the boom mass tens of meters. Using solid-state actuation, much smaller range of motion is available. Therefore, the research will have to devise actuation strategies that provide active damping of sufficient magnitude.

Previous related work by the cluster team includes development and verification via simulation of a tethered satellite yo-yo control law. In this work, we developed a nonlinear control strategy that actively damps in-plane and out-of-plane libration while maintaining continuous tension in a long, flexible tether. We have also demonstrated success in sensing and actuation using piezoelectric and shape memory alloy actuators.

Analysis

For this work, we assume the satellite is in a spherical Keplerian orbit around a spherical homogeneous earth with negligible atmosphere. Our coordinates of interest are angular disturbance (libration angle θ) and boom length l . The control variable is rate of change of boom length (\dot{l}). The system configuration is illustrated in Figure 1.1.

The equation of motion for this system, considering only pitch librational motion, can be written as³

$$\ddot{\theta} = -2\frac{\dot{l}}{l}(\dot{\theta} + \omega) - \frac{r_p \omega^2 \sin \theta}{l} \left(1 - \frac{r_p^3}{(r_p^2 + l^2 + 2r_p l \cos \theta)^{\frac{3}{2}}} \right), \quad (1.1)$$

where ω is the orbital angular velocity and the boom mass is much less than the satellite mass. For small θ , this can be simplified to³

$$\ddot{\theta} = -2\frac{\dot{l}}{l}(\dot{\theta} + \omega) - 3\omega^2 \sin \theta \cos \theta. \quad (1.2)$$

Note that if the boom length is held constant, libration frequency is independent of boom length. After being linearized, the libration frequency is approximately $\sqrt{3}\omega$. The analysis assumes that the rotational inertia of the satellite is small compared to the rotational inertia of the overall system. This can be easily achieved with a boom as short at five times the nominal satellite diameter.

A variety of control laws for this system have been devised over years. However, the yo-yo technique^{2,3} is particularly attractive in that it is model-based, exploiting two important characteristics of the librational motion. First, extending the boom when angular velocity $\dot{\theta}$ is high increases the angular moment of inertia and, via angular momentum conservation, reduces angular velocity. Second, retracting the boom when angular velocity is zero (at the extreme of θ) has no effect on angular velocity. Therefore, timing extension and retraction of the boom to the libration angle allows us to actively control angular velocity and stabilize the satellite attitude.

Control architectures

At typical Low Earth Orbit altitudes, the orbital angular velocity ω is on the order of 0.0011 rad/sec, resulting in a librational frequency of approximately 0.002 rad/sec. This frequency range is well within the frequency response capabilities of shape memory alloy actuators. A feasible boom architecture is illustrated in Figure 1.2. A simulation of satellite dynamics was developed to verify the feasibility of the architecture using yo-yo control.³ Using this architecture and with a nominal boom length of 10 meters, limiting \dot{l} to 0.015 m/sec, the satellite pitch angle was easily stabilized, as shown in Figure 1.3.

Conclusions and future work

This study has shown that active gravity gradient satellite stabilization in the orbital plane using a solid-state actuator is feasible. The next step in this work is to refine the architecture to account for SMA cooling and to refine the simulation to account for boom internal dynamics. It also will be necessary to enhance the control algorithm to account for SMA hysteresis and out-of-plane libration.

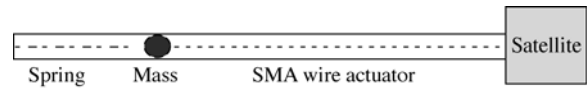


Figure 1.2. Active gravity gradient stabilization architecture

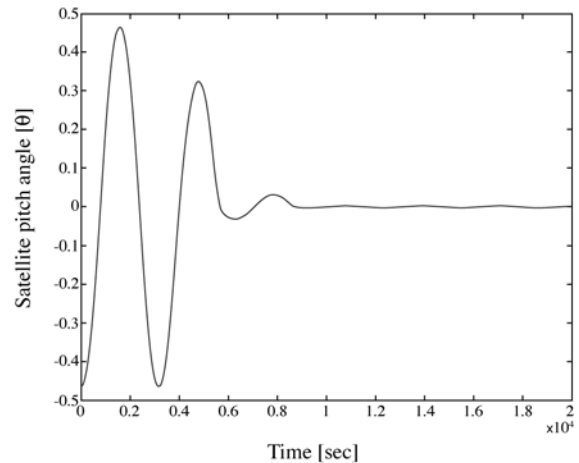


Figure 1.3. Example control results

2. INCREASING NOISE TRANSMISSION LOSS ACROSS AN ALUMINUM PANEL USING PZT ACTUATORS

Introduction

Due to its strong piezoelectric effect and high Curie point, Lead Zirconate Titanate (PZT) has become the most suitable and popular piezoceramic material. In this research, a PZT actuator along with loop shaping technique is used for the reduction of noise transmission across an aluminum panel at the modal frequencies of the panel.

Although PZT actuators have already been used by different researchers for active noise control in structures using different feedforward⁵⁻⁸ and feedback⁹⁻¹¹ techniques, these techniques have limitations. The need for a reference signal and adaptation time limit the applicability of the feedforward approach to situations with broadband, random disturbances. Modal parameters of the structure are required for designing a feedback controller for the structure, a cumbersome and time-consuming process.

Loop shaping technique for noise control was suggested by Albert et al.¹² This technique eliminates the requirement of modal parameters of the structure for controller design. Albert implemented loop shaping technique for increasing noise transmission loss across an aluminum panel using force shakers as actuators. These force shakers are large and expensive, limitations that can be addressed by using PZT actuators. The controller design and implementation have been discussed in detail.

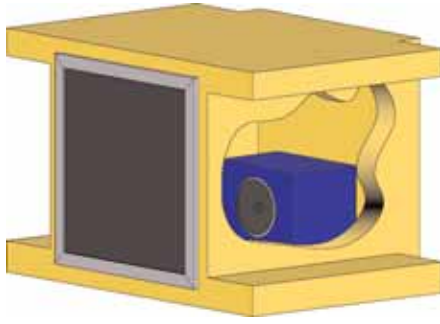


Figure 2.1. Schematic of test facility

Methodology

The aim of this research is to increase the noise transmission loss across an aluminum panel corresponding to high noise transmitting modes; that is, the odd-odd modes.¹⁰

Sensitivity is denoted as

$$S(s, \alpha) = \frac{1}{1 + L(s, \alpha)}, \quad (2.1)$$

where $L(s, \alpha) = G(s, \alpha)G_c(s)$ is the open-loop transfer function.

Sensitivity charts, which have been used to design the feedback controller for the aluminum panel in this research, relate the open-loop frequency response function of the system to the closed loop sensitivity function of the system.^{12,13} For a unity negative feedback, the sensitivity is given by

$$\begin{aligned} S(j\omega, \alpha) &= \frac{1}{1 + G(j\omega, \alpha)G_c(j\omega)} \\ &= \frac{1}{1 + L(j\omega, \alpha)}, \end{aligned} \quad (2.2)$$

where $L(j\omega, \alpha) = a(\omega, \alpha) + a(\omega, \alpha)$ is a complex function of ω . Without loss of generality, let us assume α to be implicit in the following development. The magnitude of sensitivity is given as

$$|S(j\omega)| = \frac{1}{\sqrt{(1 + a(\omega))^2 + b(\omega)^2}}. \quad (2.3)$$

Rearranging the above equation and taking the square of both sides, we get

$$[1 + a(\omega)]^2 + b(\omega)^2 = \frac{1}{|S(j\omega)|^2}. \quad (2.4)$$

Thus, for constant magnitude of sensitivity $|S(j\omega)|$, the locus of points in the complex plane is a circle with center at $(-1, j0)$ and radius $1/|S(j\omega)|$.

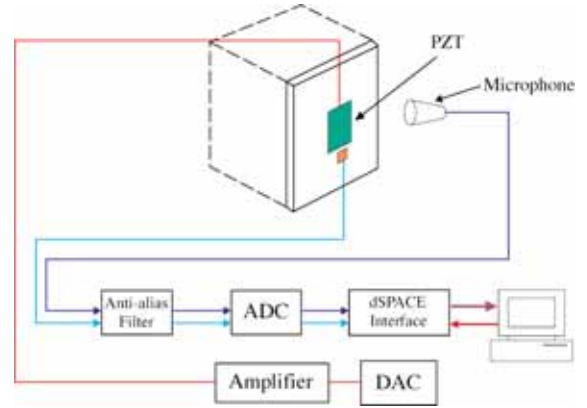


Figure 2.2. Block diagram of control system

The constant sensitivity magnitude circles are mapped to the open-loop gain phase plane using relations

$$|L(j\omega, \alpha)| = \sqrt{a(\omega)^2 + b(\omega)^2} \quad (2.5)$$

$$\angle L(j\omega) = \tan^{-1} \frac{b(\omega)}{a(\omega)}. \quad (2.6)$$

Facility description

A schematic of the test facility is shown in Figure 2.1. The setup includes a wooden box with inner dimensions 18"×18.5"×24" in the (x, y, z) directions. Five of the box walls were made of two sheets of 3/4" plywood with 4/3" of sand between the plywood sheets. The sand prevents sound transmission through the five walls. The sixth side of the box was open but framed by steel to which the panel was attached.

A block diagram of the control system is shown in Figure 2.2. The control algorithms are implemented by using the ACE 1104 board by dSPACE and softwares MATLAB, Simulink, and Real-Time Workshop.

Controller design

The targeted frequencies were selected by plotting the power spectrum of the microphone signal produced by the panel from a broadband acoustic source. The first peak is at 301.4 rad/sec and corresponds to the first modal frequency of the panel; the second peak is at 1089 rad/sec and corresponds to the fifth modal frequency of the panel.

To start with the controller design, we plot this frequency response on the sensitivity chart. The uncompensated open-loop system on the extended sensitivity chart is shown in Figure 2.3.

The objective here is to move the resonant frequencies corresponding to the first and the fifth mode of the panel to the sensitivity attenuation region. This can be achieved in three steps.

For the first part, the modal frequency of 301 rad/sec was

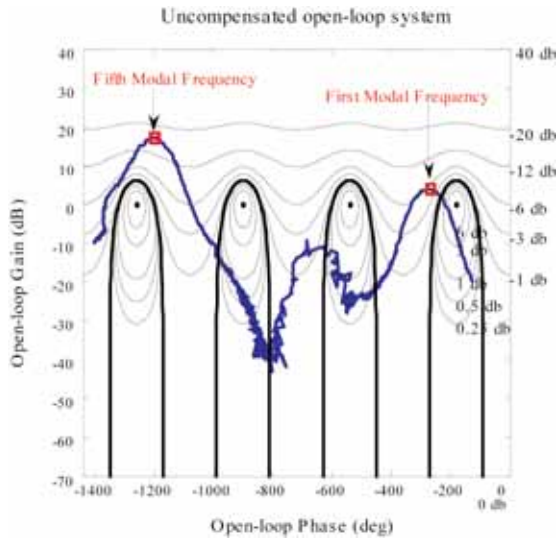


Figure 2.3. Uncompensated open-loop system on the extended sensitivity chart

pushed to the attenuation region by using a compensator, as given in the following equation.

$$\left[\frac{1}{\left(\frac{s}{310}\right)^2 + 2\frac{0.2s}{310} + 1} \right] \quad (2.7)$$

This moves the first modal frequency to the attenuation region.

$$\left[\frac{\left(\frac{s}{1069}\right)^2 - 2\frac{0.5s}{1069} + 1}{\left(\frac{s}{1069}\right)^2 + 2\frac{0.06s}{1069} + 1} \right] \quad (2.8)$$

For the fifth modal frequency, the compensator given in the above equation was chosen. The third part of the controller is a low-pass filter with cut-off frequency at 1,800 rad/sec to attenuate higher frequency components. The overall controller designed for the multimodal control of the panel is given in Equation 2.9. The compensated open-loop system on sensitivity charts using the controller is given in Figure 2.4.

$$\left[\frac{1}{\left(\frac{s}{310}\right)^2 + 2\frac{0.2s}{310} + 1} \right] \left[\frac{\left(\frac{s}{1069}\right)^2 - 2\frac{0.5s}{1069} + 1}{\left(\frac{s}{1069}\right)^2 + 2\frac{0.06s}{1069} + 1} \right] \left[\frac{1}{\frac{s}{1800} + 1} \right] \quad (2.9)$$

Performance validation

The controller design is implemented on the experimental facility, and its performance is evaluated. When this controller is implemented on the panel and excited by band-limited white noise containing the first five modal frequencies of the panel,

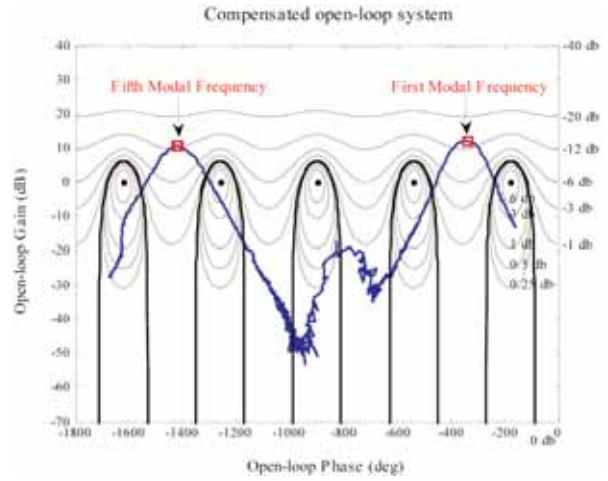


Figure 2.4. Compensated open-loop system on sensitivity charts

reduction of more than 4 dB at the first modal frequency and more than 4 dB is obtained at the fifth modal frequency. Experimental results obtained when the controller was implemented have been plotted. It can be concluded from comparison plots of uncontrolled and controlled systems that a PZT actuator has the capability of increasing noise transmission loss across the aluminum panel for multi-modes.

Conclusion

The capability of a PZT actuator to increase noise transmission loss across the panel was demonstrated for multiple modes of the panel using a single input single output (SISO) system. From the experimental results, it can be concluded that significant reductions can be achieved in noise transmission levels using PZT actuators. Moreover, the loop shaping technique for controller design can help eliminate the complex, finite element technique for system identification, or even the parametric system estimation required for modern controller designs.

3. NUMERICAL ANALYSIS OF ACOUSTIC WAVE PROPAGATION IN LAYERED CARBON NANOFIBER COMPOSITES

Introduction

Nanocomposites have attracted increasing interest in the areas of vibration suppression and acoustic damping because of their light weight, their superior mechanical response, and their stable thermal and chemical properties. Wave dispersion and attenuation in composites with uniformly distributed fillers have been extensively studied.^{14,15} Theoretical studies show that since the acoustic wavelength normally is several orders larger than the filler characteristic size in composites, Rayleigh-like scattering dominates, and the acoustic attenuation caused by nano-scale fillers is negligible due to the small scattering cross-section of individual fiber. Wave attenuation

Table 3.1. Density and mechanical property of PP, CNF-PP, and air. Note: The density of CNF-PP is an approximation.

| | $\lambda(\text{Pa})$ | $\mu(\text{Pa})$ | Density(kg/m^3) | Poisson's ratio |
|--------|---------------------------------------|---------------------------------------|-----------------------------------|-----------------|
| PP | $6.3 \times 10^8 - 4.8 \times 10^7 i$ | $2.9 \times 10^8 - 2.2 \times 10^7 i$ | 1.2×10^3 | 0.34 |
| CNF-PP | $1.7 \times 10^8 - 1.1 \times 10^8 i$ | $8.2 \times 10^8 - 5.3 \times 10^8 i$ | 1.75×10^3 | 0.34 |
| air | 1.01×10^5 | 0 | 1.2 | ---- |

due to scattering only becomes significant when the size of the inclusions in the composite is comparable to the acoustic wavelength. For audible range (20-20k Hz) acoustic waves, negligible damping effects are predicted in nanocomposites.¹⁶⁻¹⁹ Based on these theoretical predictions, most of the experimental studies on acoustic properties of nanocomposites were carried out in supersonic frequencies with shorter wavelengths.

Recently, an innovative polymer composite incorporating sheet-like carbon nanotube (CNT) or carbon nanofiber (CNF) papers has been developed.²⁰ Using these interconnected, self-supporting carbon nanostructures will significantly improve the material handling and synthesis reproducibility. As opposed to composites with uniformly distributed nanofillers, the thermal and electrical conductivity of carbon nanomaterials can be utilized. These carbon paper sheets can be arranged during polymer composite synthesis to form a layered structure consisting of stacks of polymer layer and a composite layer of CNFs saturated with polymer. Because of the drastic physical property differences in these two layers, a surface acoustic impedance gradient will be created at the interface. Acoustic wave propagation has been calculated for the normally incident wave to reveal the effects of these interfaces.

Numerical calculation results and discussion

In this research, a normal incident plane acoustic wave was considered, and the composite was described by a layered structure of two materials with infinite lateral dimensions. The acoustic wave propagated from air to the composite structure and transmitted from composite into air. The bonding between layers is assumed to be perfect. Since all plane acoustic waves can be represented by the superposition of a series of plane harmonic waves through Fourier transformation, the problem can be simplified by looking at the plane harmonic wave propagation. Our analyses are based on related theories about the wave propagation in layered structures.^{21,22} The numerical calculations based on using a polypropylene (PP) layer and nanofiber-reinforced polypropylene (CNF-PP) are shown here. Table 3.1 lists the physical properties of the two materials used in the calculations.²³ Here the Lamé's constants are expressed as complex numbers as a result of material viscoelasticity.

The interface between layers plays a critical role in the acoustic wave propagation because the acoustic impedance gradient would cause wave reflection and make the wave travel a longer distance before leaving the composite. Since the composite is viscous and absorptive, the longer distance the wave travels, the more part of the wave is absorbed. The wave speed in the PP is about 1.01×10^3 m/second, and that in the CNF-PP is around 1.39×10^3 m/second. As a result, the reflec-

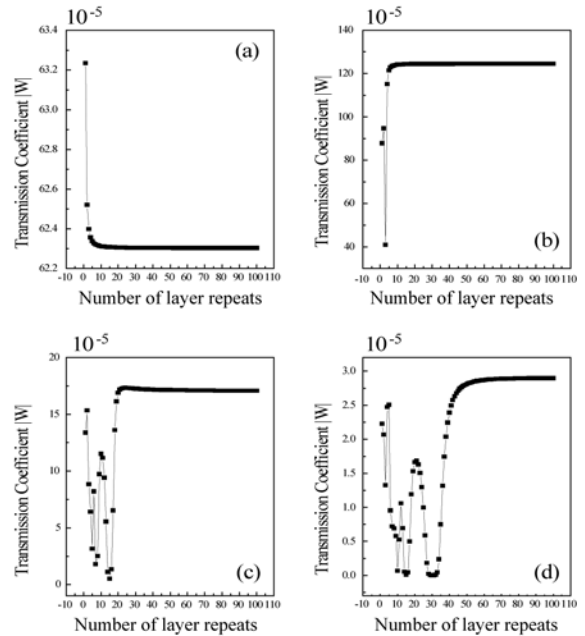


Figure 3.1. Absolute value of the un-normalized transmission coefficient vs. number of unit periods in the composite at various frequencies: (a) $\omega = 10^5$, (b) $\omega = 10^6$, (c) $\omega = 5 \times 10^6$, (d) $\omega = 10^7$

tion coefficient at the interface is approximately 0.33. Therefore, if we increase the number of alternating layers in a nanocomposite with a fixed total thickness of the two materials, the transmission coefficient is expected to decrease.

In the calculation, the total composite sample thickness is fixed at 1 cm. In each repetitive bilayer, the thickness of the PP layer is assumed to be four times that of the CNF-PP layer. For example, when $n = 1$, there is one layer of PP with a thickness of 0.002 m and one layer of CNF-PP with a thickness of 0.008 m in the composite. Figure 3.1 shows the wave transmission coefficients as a function of the number of layer repeats with different acoustic frequencies. The amplitude of the incident wave potential is set to be 10^5 , and the results for absolute value of transmission coefficients $|W|$ are not normalized. It is found that the sequence of the two phases does not influence the results.

From Figure 3.1 we can see that the introduction of the first several interfaces changes the transmission, but as the number of layer repeats increases, the transmission converges to a stable value. For frequencies corresponding to (b), (c), (d), and (e) of Figure 3.1, the transmissions oscillate with the number of unit periods at the beginning, which means that the layer structure modulates the wave propagation in an effective way and there exist some optimal configurations so that their trans-

Table 3.2. Wavelengths in pure PP and nanofiber-reinforced PP; ω : the angular frequency; λ_1 : the wavelength in PP; λ_2 the wavelength in nanofiber-reinforced PP.

| ω | 10^5 | 5×10^5 | 10^6 | 5×10^6 | 10^7 |
|-------------|--------|-----------------|--------|-----------------|--------------------|
| λ_1 | 0.06 | 0.013 | 0.006 | 0.0013 | 6×10^{-4} |
| λ_2 | 0.09 | 0.018 | 0.009 | 0.0018 | 9×10^{-4} |

missions have local minima. As more interfaces are introduced and the number of layer repeats becomes larger, the transmission varies monotonically and finally reaches a stable value. This asymptotic behavior is consistent with the theory²¹ of wave propagation through periodic, finely layered media consisting of alternating layers of two different materials. According to the theory, the acoustic absorption coefficient in such a medium only depends on the thickness ratio between the two materials when the thickness of one unit period is much smaller than the wavelengths in these two materials. In other words, when we study the wave propagation or acoustic damping in such finely layered media, the media can be modeled as effective media. The conclusion will be more evident if we compare the wavelengths at various frequencies with the thickness of the nanocomposite studied here. The wavelengths for various frequencies in two materials are listed in Table 3.2.

When angular frequency is $\omega = 10^5$, the wavelengths are much larger than the composite thickness, even before many interfaces are introduced. Therefore, in the transmission illustrated in Figure 3.1 (a), the coefficient does not experience oscillation and settles to a stable value that quickly converges to the initial transmission value. When the angular frequency is so large that the wavelengths are comparable to or smaller than the sample thickness, the transmission oscillates at the beginning and then settles to a stable value as the number of layer repeats becomes large where the thickness of one repeat unit is much smaller than the wavelengths. It is inferred by Figure 3.1 that the critical number of layer repeats that initializes the stable transmission increases with the frequency.

Table 3.3 shows the respective critical number and the ratio of corresponding thickness of one unit period to the averaged wavelength. It is evident that the thicknesses are much less than the averaged wavelength.

We also simulated the wave propagation through nanocomposite by considering the nanocomposite as a homogeneous effective medium with the effective Lamé's constants and the effective density weighted on volume fractions. Here the volume fractions of pure PP and CNF PP are 80 percent and 20 percent, respectively. The calculated transmission coefficients of the effective media for different angular frequency are shown in Figure 3.2, recalling that in Figure 3.1, for each frequency there is a stable value for the transmission coefficient when the number of unit periods becomes large. If we compare the stable transmission coefficient for each frequency in Figure 3.1 with the corresponding transmission coefficient for the same frequency in Figure 3.2, it is evident that every two corresponding transmission coefficients are very close. The coincidence of the data for the transmission coefficient calculated from the above two methods confirms that when we

Table 3.3. Critical numbers of layer repeats and their ratios to the averaged wavelengths; ω : the angular frequency; n_c the critical number of layer repeats; h : the thickness of one layer repeat.

| ω | n_c | $h(m)$ | $2h/(\lambda_1 + \lambda_2)$ |
|-----------------|-------|----------------------|------------------------------|
| 10^6 | 7 | 1.4×10^{-3} | 18% |
| 5×10^6 | 20 | 5.0×10^{-4} | 30% |
| 1×10^7 | 50 | 2.0×10^{-4} | 26% |

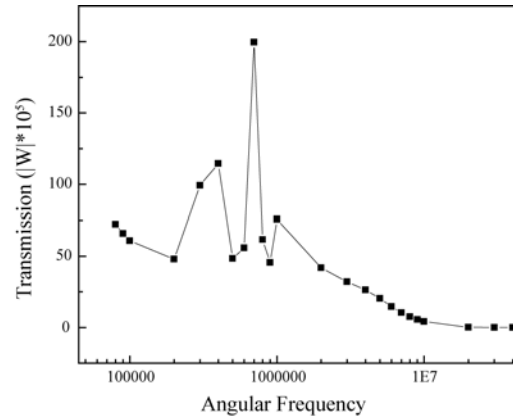


Figure 3.2 The un-normalized transmission coefficient is calculated as the function of angular frequency for effective media.

study the wave propagation and the acoustic damping in layered nanocomposite, the composite can be modeled as a homogeneous effective medium if its thickness of one unit period is much smaller than the wavelengths.

Conclusion

In this section, we studied the normally incident plane harmonic acoustic wave propagating through layered nanocomposites. The transmission coefficients were calculated to show that there exist some optimal configurations for layered structures so that the transmission coefficients can have local minima. When the thickness of one unit period in nanocomposite is much smaller than the wavelengths, the wave propagation and acoustic damping can be studied by considering the layered nanocomposite as a homogeneous effective medium.

4. FUZZY LOGIC-BASED ACTIVE VIBRATION CONTROL OF A SMART BEAM WITH MASS UNCERTAINTY

Introduction

Increasing attention has been given recently to vibration control of lightly damped, flexible structures (satellites, towers) using piezoceramic material. Applications have been studied in the areas of aeronautical and mechanical engineering, as well as in civil engineering. The advantages of piezoceramic material include low power consumption, the absence of moving

parts, quick response, compactness, and easy implementation.

There have been many promising results in the vibration control study of flexible structures using piezoceramic materials. Andreus (2004) designed a novel passive device for multimodal structural vibration damping based on distributed piezoelectric controllers for engineering applications.²⁴ Sharma et al. (2005) have developed a fuzzy logic-based independent modal space controller and a fuzzy logic-based modified independent modal space controller for the vibration control of a cantilevered beam.²⁵ Choi (2006) has developed a robust vibration control approach for a smart beam structure featuring piezoceramic actuators.²⁶ Lin and Liu (2006) developed a novel resonant fuzzy logic controller to minimize structural vibration using collocated piezoelectric actuator/sensor pairs through experimental study.²⁷ Song and Gu (2007) proposed a robust sliding mode control for active vibration control of flexible beam. Their experiment demonstrated that the proposed controller outperformed the PD control and lead compensation for the suppression of vibration.²⁸ Song and Gu (2007) also presented a robust model reference controller that has the ability to handle model uncertainties for active vibration suppression of a flexible beam with a piezoceramic sensor and actuator.²⁹ Suhariyono et al. (2008) used a lightweight piezo-composite actuator to suppress the vibration of an aluminum beam with a PID controller.³⁰

Model uncertainties are inevitable in actual engineering and require the controller to be either adaptive or robust to these. In this chapter, the experimental study of different fuzzy controllers was performed on an aluminum beam instrumented with two piezoelectric patches mounted close to the clamped end. General fuzzy controllers with different fuzzy inputs were applied to control the vibration of beam. In order to guarantee the robustness of the controller, the adaptive fuzzy sliding-mode (AFSM) control is proposed to deal with the model uncertainty. All the controllers above were tested considering different additional masses as mass uncertainty to verify the corresponding robustness. Furthermore, AFSM control was tested under earthquake excitation. Experimental results were analyzed deeply and show the robustness and effectiveness of the presented controllers in this report.

Design of adaptive fuzzy sliding-mode controller

Consider the uncertain beam as the general nonlinear differential equation

$$\ddot{x} = f(x, \dot{x}) + \bar{u} + \bar{d}, \quad (4.1)$$

where $f(x, \dot{x})$ denote the properties of the beam, \bar{u} is the control input, and \bar{d} is the unknown external excitation.

The control force of adaptive fuzzy sliding-mode control is given by sliding-mode control. According to the arrival condition and the definition of sliding surface, the sliding-mode control force and sliding surface can be obtained as

$$\bar{u} = -c_1 \dot{x} - f(x, \dot{x}) - (D + \eta) \text{sgn}(s) \quad (4.2)$$

$$s = -c_1 x + \dot{x}, \quad c_1 > 0, \quad (4.3)$$

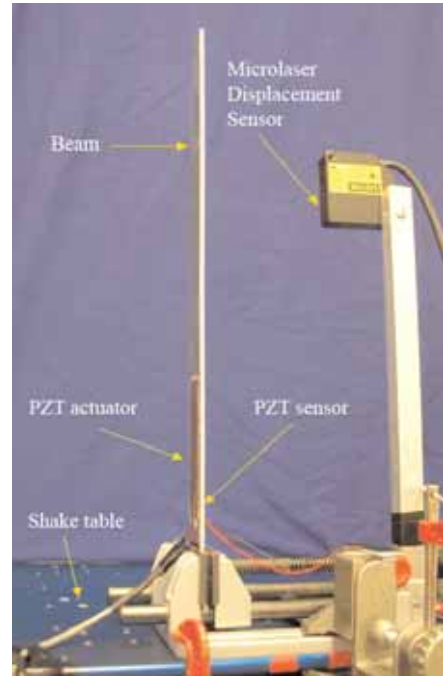


Figure 4.1. The experimental setup

where c_1 is a positive constant; η is the adjustable parameter of arrival condition; $f(x, \dot{x})$ represents the characteristic of nonlinear structure; D is the upper limit of external excitation; and s is the sliding surface.

Because $f(x, \dot{x})$ is unknown, the control force shown in Equation 4.2 cannot be realized. The reasonable consideration is to substitute $f(x, \dot{x})$ by the fuzzy system $\hat{f}(\mathbf{x}|\theta_f)$ so that the sliding-mode control can be used without the characteristics of a nonlinear structure beforehand. Moreover, the nonlinear term $(D + \eta) \text{sgn}(s)$ in the control law yields too many switches in the sliding surface and leads to chattering phenomenon. Thus, the other fuzzy system $\hat{f}(s|\theta_s)$ is introduced to substitute the nonlinear term. Then Equation 4.2 can be rewritten as

$$\bar{u} = -c_1 \dot{x} - \hat{f}(\mathbf{x}|\theta_f) - \hat{f}(s|\theta_s). \quad (4.4)$$

Then, based on Lyapunov stability theory, we can obtain the adaptation law as

$$\dot{\theta}_f = \gamma_1 s \xi(\mathbf{x}) \quad (4.5)$$

$$\dot{\theta}_s = \gamma_2 s \Psi(s). \quad (4.6)$$

Experimental setup

The experimental object was an aluminum beam in a cantilevered configuration, as shown in Figure 4.1. PZT-type piezoelectric ceramic patches were used as the smart sensor and actuator. The sensor signal was acquired by and the control signal was also sent out by a dSPACE data acquisition board. A signal amplifier was used to amplify the control signal so as to drive the PZT actuator. Furthermore, a shaker table was used to generate the earthquake excitation. In the hosting

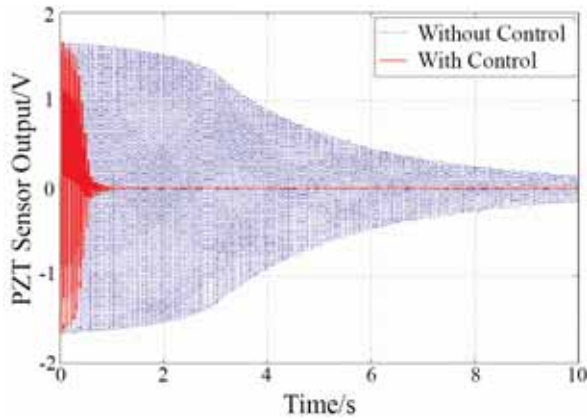


Figure 4.2. AFSM control based on PZT sensor

computer, the dSPACE ControlDesk module was used to develop a graphical user interface for real-time control and data acquisition.

Experimental result

Without mass uncertainty. At first, the beam without mass uncertainty was accepted as a control objective, and adaptive fuzzy sliding-mode control was applied to this beam. Figure 4.2 shows the comparison data with and without control. The experimental results show that AFSM control works very well under the case without mass uncertainty.

Additional mass: 10 g. In order to verify the robustness of the above controllers, an additional mass of 10 g was added to the tip of the beam, approximately a 31 percent increase in the total effective mass. Here, effective mass was defined as the mass in the tip of the beam, which is equivalent to the distributed mass of the beam in the sense of dynamic characteristics.

Figure 4.3 shows the results with AFSM control. From the control results, we can see that AFSM control retains the level of effectiveness as without additional mass.

Conclusion

In this report, the experimental study of the vibration control of a beam was conducted using fuzzy logic controllers. Additional masses were added to the tip of a beam to simulate model uncertainty. Both the general fuzzy controller and the AFSM controller were tested with different additional masses. Furthermore, the AFSM controller was also applied to control the vibration of a beam under earthquake excitation with mass uncertainties. Based on the experimental results, the following conclusions can be drawn:

1. Considering the general fuzzy controller, the fuzzy input directly affects the fuzzy control objective. If the displacement of the beam is accepted as the fuzzy input, better results will be obtained than with PZT output acting as the fuzzy input. Furthermore, increasing the number of fuzzy inputs will also lead to better control effects.
2. With low mass uncertainty, the general fuzzy controller can

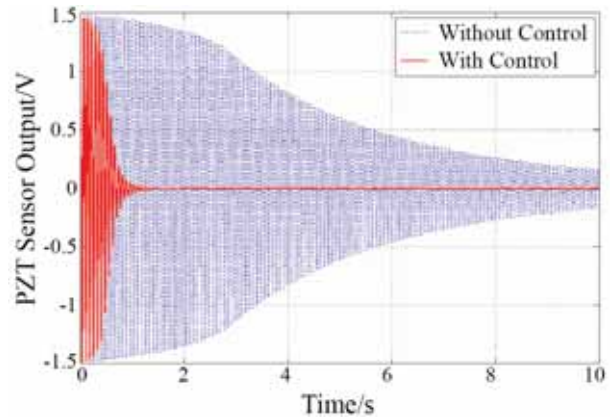


Figure 4.3. AFSM control based on PZT sensor

control the vibration of the beam. However, when the mass uncertainty was too high, the general fuzzy controller was not particularly effective in suppressing the beam's vibration. On the other hand, the AFSM controller, which can deal with model uncertainties, worked very well with different mass uncertainties.

3. The AFSM controller also controlled the vibration of a beam under earthquake excitation satisfyingly with mass uncertainties through experimental study.

5. ACTIVE VIBRATION OF A SMART BEAM

Introduction

An imperative need exists to develop an effective approach to active vibration control for flexible structures in the aerospace industry and beyond. Vibration is a major concern in a variety of engineering fields and, in general, its effects are considered deleterious. Research has long been devoted to the suppression of vibration in these lightweight and under-damped structures, yet the development of innovative smart materials and their potential for the aerospace industry has lent new intensity to research in this area.

Recently, different innovative vibration control strategies have been developed for the active vibration control of flexible structures.³¹⁻³⁸ This section describes how an interactive smart vibrating beam (SVB) was developed with a low-cost, Freescale MC9S12C32 microcontroller to demonstrate vibration at different natural modal frequencies. This served as a vibration control object for positive position feedback control and sliding mode control.

In this SVB experimental setup, piezoceramic materials were used as an actuator and a sensor. Piezoceramic sensors and actuators are widely used in vibration suppression because they are lightweight, responsive, and solid-state. The smart beam has two surface-bonded PZT patches, one as an actuator and the other as a sensor. An interactive user interface with LCD display, keypad, and push buttons was also developed. Through the use of buttons, the microcontroller excites the

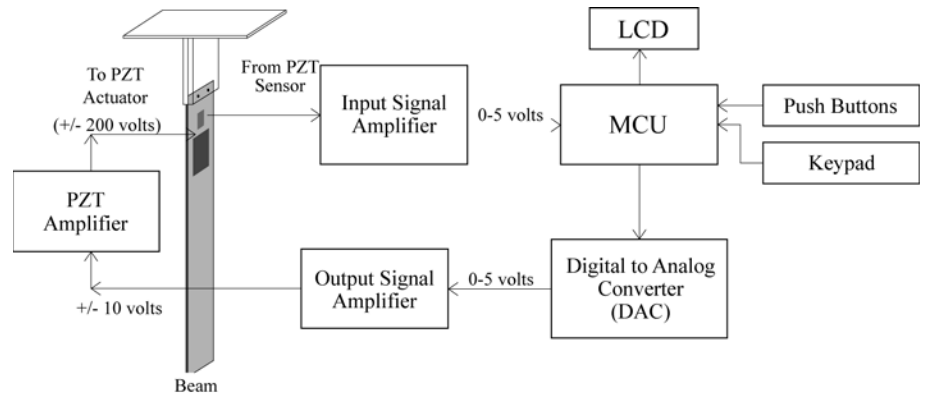
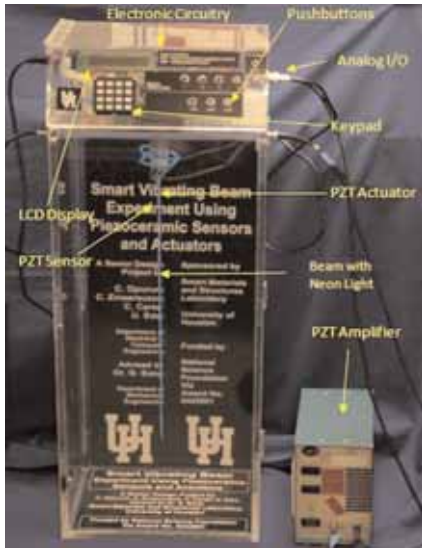


Figure 5.1. (left) Experimental setup

Figure 5.2. (above) Block diagram of the setup of the smart vibrating beam

beam at the first four modal frequencies and also controls the first modal vibration of the beam using PPF control and sliding mode control. The keypad can be used to input a customized excitation frequency value, ranging from 0.1 Hz to 400 Hz.

Experimental setup of the SVB

Figure 5.1 of the experiment shows a cantilevered, vertically mounted aluminum beam with a neon light attached to the edges for better display of mode shapes. A block diagram of the setup of the smart vibrating beam is shown in Figure 5.2. Two PZT patches were attached on each side of the beam; one was used as an actuator (P1-8528) and the other as a sensor (QP 10s). The beam properties and PZT actuator and sensor properties are given in Table 5.1 and Table 5.2, respectively. The beam structure was enclosed in a transparent acrylic box. All electronic circuitry was placed in another such box on top.

Electronic circuitry

To control the smart vibrating beam experiment, an electronic circuit was designed to excite the vibration with a sinusoidal signal of specific frequency and to suppress vibration of the first dominant mode of the beam with positive positioning feedback controller (PPF) and sliding mode controller (SMF). The brain of the circuitry was the CML12C32 evaluation board from Axiom. The evaluation board incorporates an 8-bit A/D converter and is interfaced with a liquid crystal display, a keypad, and seven push buttons. The keypad and pushbuttons are used to select the frequency of excitation and to suppress the vibration with the signal from the microcontroller. For signal conditioning of the sensor signal and actuator signal, two signal conditioning and amplifier circuits were developed. One circuit was for the sensor signal and other for the actuator signal.

The digital output signal from the microcontroller was converted to an analog signal by using an 8-bit digital-to-analog converter. The output from the D/A converter was conditioned

to +/- 10 volts with the output signal amplifier. This actuation signal was then fed into an external PZT amplifier that amplifies the signal to +/- 200 volts, and the output signal from the PZT amplifier was fed to PZT actuator.

The microcontroller reads the analog signal from the PZT sensor at the customized sampling frequency of 1,000 Hz. The sensor signal was conditioned with an input signal amplifier to the voltage range of 0-5 volts and fed to A/D converter.

Functions of microcontroller in SVB

The microcontroller was used to generate waves to excite the vibration, process the sampled data from the sensor, and control the first mode vibration by using PPF and sliding mode

Table 5.1. Beam properties

| Symbol | Quantity | Units | Value |
|--------|--------------|-------------------|-----------------------|
| L | Length | (mm) | 529.9 |
| W | Width | (mm) | 48.7 |
| T | Thickness | (mm) | 0.68 |
| ρ | Beam density | Kg/m ³ | 2690 |
| E | Y. Modulus | N/m ² | 7.03×10^{10} |

Table 5.2. PZT actuator and sensor properties

| Symbol | Quantity | Units | PZT Actuator | PZT Sensor |
|-----------------|---------------|-------------------|------------------------|------------------------|
| L | Length | (mm) | 72.3×28×0.12 | 12.7×6.35×0.25 |
| w | Width | (mm) | 28 | 6.35 |
| t | Thickness | (mm) | 0.12 | 0.25 |
| d ₃₃ | Strain Coeff. | (C/N) | 4×10^{-10} | 3.5×10^{-10} |
| d ₃₁ | Strain Coeff. | (C/N) | 1.79×10^{-10} | 1.79×10^{-10} |
| ρ_p | PZT density | Kg/m ³ | 7300 | 7700 |
| E | Young Modulus | N/m ² | 3.3×10^{10} | 6.9×10^{10} |

control algorithms. The microcontroller code, written in C, performs the following functions:

- Monitoring user interface
- Exciting different modes of vibration
- Controlling vibration

User interface. The user interface includes initializing the LCD and monitoring the keypad and push buttons for vibration excitation and vibration suppression. The selection options, such as frequency of excitation and choice of controller, and exiting of the vibration mode, are shown on the LCD.

Excite different modes of vibration. For vibration excitation, a sinusoidal signal of desired frequency was generated from the microcontroller. The microcontroller uses an array of 256 elements, which defines a period of a sinusoidal wave. Each element of the array was 8-bit. An interrupt subroutine was called by selecting the frequency, which initializes a counter and resets itself after reaching a certain value depending on the desired frequency. Each time the counter resets itself, the microcontroller sends one element from the sinusoidal array to the output port. The digital output signal was then converted to an analog signal and used to excite the vibration of the beam. After sending 256 elements, the microcontroller restarts from the first element and, thus, generates a sinusoidal signal of the selected frequency.

Control vibration. For the first modal vibration suppression of the smart beam, PPF control and sliding mode control algorithms were implemented on the microcontroller. The basic theory and control implementation of these algorithms are given below.

PPF control. The compensator is composed of a second-order filter with the same form of transfer function as that in the system, but with a much higher damping ratio. To achieve maximum damping, ω_c , the compensator's natural frequency, should be closely matched with ω , the system's natural frequency.

Sliding mode control. The typical sliding-mode controller is composed of estimation terms of the system to approximate the system dynamics and a robust compensator, which deals with model uncertainty and disturbance to ensure stability. The robust compensator usually consists of an upper bounding of the system uncertainty with a discontinuous mathematical function, such as a sign function or a saturation function. Here, the tangent hyperbolic function was used as a robust compensator. The equations for the sliding mode controller are as follows:

$$e(t) = y(t) - y_d(t) \quad (5.1)$$

$$s = e(t) + \lambda e(t) \quad (5.2)$$

$$u(t) = -K_d s - \rho \tanh(\alpha s), \quad (5.3)$$

where $y(t)$ is the sensor output, $y_d(t)$ is the set point, s is the sliding surface, and $u(t)$ is the control action. The control gains are $\lambda > 0$ and the constants $K_d > 0$ and $\rho > 0$.



Figure 5.3. First mode



Figure 5.4. Second mode

Steps for SVB experiment

For SVB experiments, the user needs to go through the following steps:

Enter the frequency of vibration through keypad (between frequencies ranging from 0.1-400 Hz) or push buttons (modal vibrations).

1. If the entered frequency is equal to the first modal vibration, select the control algorithm between PPF and sliding mode control for vibration suppression by pressing the respective button.
2. To exit from vibration mode or control mode, press “Exit” or “D” on the keypad.

Testing of smart vibrating beam

The smart vibrating beam was tested for vibration excitation at specified frequency and for vibration suppression of the first modal vibration with PPF control and sliding mode control. Figure 5.3 and Figure 5.4 have shown the first and second modal vibrations of the beam.

From the experimental results shown in Figure 5.5 and Figure 5.6, the first modal vibration was suppressed using the PPF control algorithm and the sliding mode control algorithm.

Conclusions

In this chapter, a smart vibrating beam experimental setup (SVB) was developed to demonstrate vibration phenomena and vibration control techniques. The vibration of the beam was excited by actuating the PZT actuator with the amplified signal from the microcontroller. For vibration control demonstration, two control algorithms—PPF and sliding mode control—were implemented on the flexible beam. The SVB experiment involved a multifunctional platform, where vibration of the beam could be excited for the frequency range of 0-400 Hz, and the first modal vibration was successfully suppressed by using the PPF control algorithm and sliding mode control. The experimental results have shown that compared to the 2 percent damping ratio of the uncontrolled system, the

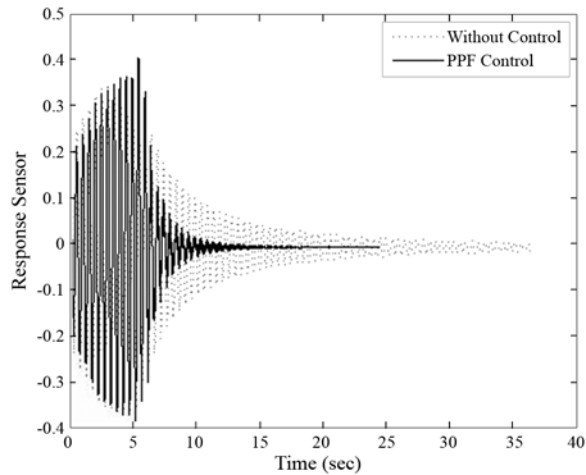


Figure 5.5. Comparison of vibration suppression with PPF control and free vibration

damping ratio was increased to 4.98 percent using PPF control and 5.18 percent using sliding mode control.

6. CONCLUSIONS

This report presents the joint research conducted by the central campus and Clear Lake campus of the University of Houston on solid state actuators, such as piezoceramics, and their applications in acoustic and vibration reduction. Several conclusions can be drawn from this study.

1. Active gravity gradient satellite stabilization in the orbital plane using a solid-state actuator is feasible.
2. The capability of piezoceramic actuators, along with the loop shaping technique, has been shown to increase noise transmission loss across an aluminum panel corresponding to the modal frequencies for broadband excitations of the panel.
3. The normally incident plane harmonic acoustic wave propagating through layered nanocomposites was studied. The transmission coefficients were calculated to show that there exist some optimal configurations for the layered structures so that the transmission coefficients can have local minima.
4. The effectiveness of the proposed fuzzy logic controller is experimentally verified under mass uncertainty.
5. A smart vibration beam experimental setup for both research and education was developed and two types of active vibration control approaches—PPF and sliding mode controls—were implemented.

REFERENCES

1. Martinelli, M.I. and Sanchez Pena, R.S. Passive 3 axis attitude control of MSU-1 pico-satellite. *Acta Astronautica* **56**, 507-517 (2005).
2. Davis, W.R. and Banerjee, A.K. Librational damping of a tethered satellite by yo-yo control with angle measurement, *J. Guidance* **13**, 370-374 (1990).
3. Dabney, J.B., Hasdorff, L., Harman, T.L., and Watson, J.T. Effects of tether stretch dynamics on a tethered satellite yo-

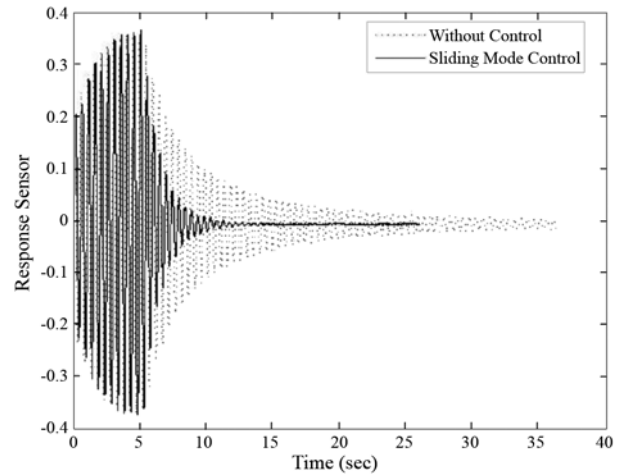


Figure 5.6. Comparison of vibration suppression with Sliding Mode control and free vibration

yo control law. Joint Applications in Instrumentation Processes and Computer Control, Houston, TX, March 26 (1993).

4. Nashif, A.D. Control of noise and vibration with damping materials. *Sound and Vibration* **17**, 28-36 (1983).
5. Rossetti, D.J. and Norris, M.A. A comparison of actuation and sensing techniques for aircraft cabin noise control. *Noise Control Engineering Journal* **44**, 53-58 (1996).
6. Clark, R.L. and Fuller, C.R. Control of sound radiation with adaptive structures. *J. Intelligent Material Systems and Structures* **2**, 431-452 (1991).
7. Balachandran, B. and Sampath, A. Studies on active acoustics control. *Proceedings of the SPIE—The International Society for Optical Engineering* **3321**, 378-389 (1998).
8. Fuller, C.R. Active control of sound transmission/radiation from elastic plates by vibration inputs: I. Analysis. *J. Sound and Vibration* **136**, 1-15 (1990).
9. Savran, C.A., Atalla, M.J., and Hall, S.R. Broadband active structural-acoustic control of fuselage test-bed using collocated piezoelectric sensors and actuators. *Proceedings of the SPIE—The International Society for Optical Engineering* **3984**, 136-147 (2000).
10. Niekerk, J.L.V., Tongue, B.H., and Packard, A.K. Active control of a circular plate to reduce transient noise transmission. *J. Sound and Vibration* **183**, 643-662 (1995).
11. Bevan, J.S. and Mei, C. Piezoceramic actuator placement for structural acoustic and vibration control of flat and curved panels. *Proceedings of the SPIE—The International Society for Optical Engineering* **4327**, 698-708 (2001).
12. Albert, D.S., Francheck, M.A., and Bernhard, R.J. Active control of transmission loss in lightly damped panels. *Noise Control Engineering Journal* **48**, 48-59 (2000).
13. Sethi, V., Song, G., and Francheck, M.A. Loopshaping control of a model story building using smart materials. *Proceedings of the 2nd International Conference on Structural Health Monitoring of Intelligent Infrastructure*, Shenzhen, China (2005).



VIBRATION—Mithun Singla (left), M.S. student in electrical and computer engineering, and Gangbing Song (right), director of the Smart Materials and Structures Laboratory, have experimented with two types of active vibration controls: PPF and sliding mode.

14. Yang, C.F. and Truell, R. Scattering of a plane longitudinal wave by a spherical obstacle in an isotropically elastic solids. *J. Applied Physics* **27**, 1086 (1956).
15. Morse, P.M. and Ingard, K.U. *Theoretical Acoustics*. (Princeton University Press, 1986).
16. Foldy, L.L. The multiple scattering of waves I. General theory of isotropic scattering by randomly distributed scatterers. *Physical Review* **67**, 107-119 (1945).
17. Lax, M. Multiple scattering of waves. II The effective field in dense systems. *Physical Review* **85**, 621-629 (1952).
18. Waterman, P.C., and Truell, R. Multiple scattering of waves. *J. Mathematical Physics* **2**, 512 (1961).
19. Verbis, J.T., Kattis, S.E., Tsinopoulos, S.V., and Polyzos, D. Wave dispersion and attenuation in fiber composites. *Computational Mechanics* **27**, 244-252 (2001).
20. Gou, J., O'Braint, S., Gu, H.C., and Song, G.B. Damping augmentation of nanocomposites using carbon nanofiber paper. *J. Nanomaterials*, article ID 32803, 1-7 (2006).
21. Brekhovskikh, L.M. *Waves in Layered Media*. (Academic, New York, 1980).
22. Bedford, A., and Drumheller, D.S. *Introduction to Elastic Wave Propagation*. (Wiley, New York, 1994).
23. Finegan, I.C., Tibbetts, G.G., and Gibson, R.F. Modeling and characterization of damping in carbon nanofiber/polypropylene composites. *Composites Science and Technology* **63**, 1629-1635 (2003).
24. Andraus, U., Dellisola, F., and Porfiri, M. Piezoelectric passive distributed controllers for beam flexural vibration. *J. Vibration and Control* **10**, 625-659 (2004).
25. Sharma, M., Singh, S.P., and Sachdeva, B.L. Fuzzy logic based modal space control of a cantilevered beam instrumented with piezoelectric patches. *Smart Materials and Structures* **14**, 1017-1024 (2005).
26. Choi, S.B. Vibration control of a smart beam structure subjected to actuator uncertainty: Experimental verification. *Acta Mechanica* **181**, 19-30 (2006).
27. Lin, J. and Liu, W.Z. Experimental evaluation of a piezoelectric vibration absorber using a simplified fuzzy controller in a cantilever beam. *J. Sound and Vibration* **296**, 567-582 (2006).
28. Song, G. and Gu, H. Active vibration suppression of a smart flexible beam using a sliding mode based controller. *J. Vibration and Control* **13**, 1095-1107 (2007).
29. Gu, H. and Song, G. Active vibration suppression of a flexible beam with piezoceramic patches using robust model reference control. *Smart Materials and Structures* **16**, 1453-1459 (2007).
30. Suhariyono, A., Goo, N.S., and Park, H.C. Use of lightweight piezo-composite actuators to suppress the free vibration of an aluminum beam. *J. Intelligent Material Systems and Structure* **19**, 101-112 (2008).
31. Passino, K.M. and Yurkovich, S. *Fuzzy Control*. (Addison Wesley Longman, Inc, 1998).
32. Fanson, J.L. and Caughey, T.K. Positive position feedback control for large space structures. *AIAA J.* **28**, 717-724 (1990).
33. Song, G., Qiao, P., Sethi, V., and Prasad, A. Active vibration control of a smart pultruded fiber reinforced polymer I-beam. *Proceedings of SPIE International Symposium on Smart Structures and Materials*, San Diego, CA (2002).
34. Kar, I.N., Seto, K., and Doi, F. Multimode vibration control of flexible structure using H-infinity based robust control. *IEEE/ASME Trans. on Mechatronics* **5**, 23-31 (2000).
35. Corr, L.R. and Clark, W.W. A novel semi-active multimodal vibration control law for piezoceramic actuator. *J. Vibration and Acoustics* **125**, 214-222 (2003).
36. Rew, K.H., Han, J.H., and Lee, I. Multimodal vibration control using adaptive positive position feedback. *J. Intelligent Mater. Systems and Struc.* **13**, 13-22 (2002).
37. Han, J.H., Rew, K.H., and Lee, I. An experimental study of active vibration control of composite structures with a piezo ceramic actuator and a piezo film sensor. *Smart Mater. and Struc.* **6**, 549-558 (1997).
38. Prakah-Asante, K.O. and Craig, K.C. The application of multi-channel design methods for vibration control of an active structure. *Smart Mater. and Struc.* **3**, 329-343 (1994).
39. Sethi, V. and Song, G. Multimodal vibration control of a flexible structure using piezoceramics. International Conference on Advance Intelligent Mechatronics, Monterey, CA (July 24–25, 2005).